

Creation of highly aligned electrospun poly-L-lactic acid fibers for nerve regeneration applications

Han Bing Wang¹, Michael E Mullins¹, Jared M Cregg²,
Andres Hurtado^{3,4}, Martin Oudega^{3,4}, Matthew T Trombley²
and Ryan J Gilbert²

¹ Department of Chemical Engineering, Michigan Technological University, Houghton, MI 49931, USA

² Regeneration and Repair Laboratory, Department of Biomedical Engineering, Michigan Technological University, Houghton, MI 49931, USA

³ International Center for Spinal Cord Injury, Hugo W Moser Research Institute at Kennedy Krieger, Baltimore, MD 21205, USA

⁴ Department of Neurology, Johns Hopkins University School of Medicine, Baltimore, MD 21205, USA

E-mail: rgilbert@mtu.edu

Received 25 November 2008

Accepted for publication 25 November 2008

Published 22 December 2008

Online at stacks.iop.org/JNE/6/016001

Abstract

Aligned, electrospun polymer fibers have shown considerable promise in directing regenerating axons *in vitro* and *in vivo*. However, in several studies, final electrospinning parameters are presented for producing aligned fiber scaffolds, and alignment where minimal fiber crossing occurs is not achieved. Highly aligned species are necessary for neural tissue engineering applications to ensure that axonal extension occurs through a regenerating environment efficiently. Axonal outgrowth on fibers that deviate from the natural axis of growth may delay axonal extension from one end of a scaffold to the other. Therefore, producing aligned fiber scaffolds with little fiber crossing is essential. In this study, the contributions of four electrospinning parameters (collection disk rotation speed, needle size, needle tip shape and syringe pump flow rate) were investigated thoroughly with the goal of finding parameters to obtain highly aligned electrospun fibers made from poly-L-lactic acid (PLLA). Using an 8 wt% PLLA solution in chloroform, a collection disk rotation speed of 1000 revolutions per minute (rpm), a 22 gauge, sharp-tip needle and a syringe pump rate of 2 ml h⁻¹ produced highly aligned fiber (1.2–1.6 µm in diameter) scaffolds verified using a fast Fourier transform and a fiber alignment quantification technique. Additionally, the application of an insulating sheath around the needle tip improved the rate of fiber deposition (electrospinning efficiency). Optimized scaffolds were then evaluated *in vitro* using embryonic stage nine (E9) chick dorsal root ganglia (DRGs) and rat Schwann cells (SCs). To demonstrate the importance of creating highly aligned scaffolds to direct neurite outgrowth, scaffolds were created that contained crossing fibers. Neurites on these scaffolds were directed down the axis of the aligned fibers, but neurites also grew along the crossed fibers. At times, these crossed fibers even stopped further axonal extension. Highly aligned PLLA fibers generated under optimized electrospinning conditions guided neurite and SC growth along the aligned fibers. Schwann cells demonstrated the bipolar phenotype seen along the fibers. Using a novel technique to determine fiber density, an increase in fiber density correlated to an increase in the number of neurites, but average neurite length was not statistically different between the two different fiber densities. Together, this work presents methods by which to produce highly

aligned fiber scaffolds efficiently and techniques for assessing neurite outgrowth on different fiber scaffolds, while suggesting that crossing fibers may be detrimental in fostering efficient, directed axonal outgrowth.

(Some figures in this article are in colour only in the electronic version)

1. Introduction

The development of novel scaffolds able to guide axonal growth is important to facilitate axonal regeneration through injured environments in the peripheral nervous system (PNS) and central nervous system (CNS). The material should be biocompatible and closely resemble native extracellular matrix environments that neurons use to guide axonal extensions during development; it should also be degradable so that the scaffold degrades as axons grow through the injury site. The mechanical properties of the material are also an important parameter as tough, rigid materials may induce additional damage following implantation and/or make it difficult for regenerating axons to penetrate into the material (Balgude *et al* 2001)

Although the desired properties of a neural scaffold, such as biodegradability, biocompatibility and biomechanical character, have been extensively studied, creating a system that satisfies all such properties remains elusive. Recently, others have used novel fabrication techniques to design materials that guide axonal outgrowth. Aligned conduits (Hadlock *et al* 2000, Stokols and Tuszyński 2006), fibers/filaments (Chauhan *et al* 1999, Rangappa *et al* 2000, Ngo *et al* 2003, Cai *et al* 2005, Wen *et al* 2006, Schnell *et al* 2007, Corey *et al* 2007, 2008, Kim *et al* 2008) and hydrogels (Ceballos *et al* 1999, Luo *et al* 2004, Prang *et al* 2006, Dodla and Bellamkonda 2006, 2008) which facilitate directed growth of axons *in vitro* and *in vivo* have all shown promise in assisting axonal extension in a directed manner. However, there is no standard material or fabrication technique that is generally accepted as being optimum for facilitating directional outgrowth. Thus, further development of novel scaffolds is necessary.

Electrospinning is increasingly being investigated to create scaffolds for tissue engineering applications. In neural tissue engineering, the longitudinal distribution of axons in both the CNS and the PNS makes it imperative to design scaffolds able to guide regenerating axons along their natural axis of growth. To date, *in vitro* experiments using rat DRGs on PLLA (Corey *et al* 2007) or poly(acrylonitrile-co-methylacrylate (Kim *et al* 2008), chick DRGs on poly- ϵ -caprolactone (Schnell *et al* 2006), neural stem cells on PLLA (Yang *et al* 2004, 2005) and primary motor neurons (from spinal cord) and sensory neurons (from DRGs) from rat on PLLA (Corey *et al* 2008) have demonstrated the ability of aligned fibers to facilitate directed neurite outgrowth in comparison to randomly oriented fiber species. Further, aligned, electrospun fibers have shown promise in fostering robust regeneration *in vivo* within a rat peripheral nerve injury model either without neurotrophin (Kim *et al* 2008) or with

neurotrophin (Chew *et al* 2007). While fibers in these studies were more aligned than randomly oriented fibers, a number of fibers still crossed. Crossing fibers are significant since they may restrict or divert axonal outgrowth from occurring down the longitudinal axis of the implant. Therefore, manipulation of electrospinning parameters is essential to produce highly aligned fiber species that facilitate nerve regeneration through an injury site as quickly and as efficiently as possible.

In this study, electrospinning parameters have been manipulated to produce highly aligned fiber specimens by manipulating four electrospinning parameters: the rotation speed of the collection disk, the needle size, the needle tip shape and the syringe pump flow rate. A novel insulating sheath was introduced to the needle tip to increase electrospinning efficiency. Samples were imaged using scanning electron microscopy (SEM) and the fiber density and alignment were characterized. A novel procedure for determining fiber density was established. E9 chick DRG explants and rat SCs were cultured on optimized scaffolds that contained aligned fibers at two different densities, respectively. By manipulating electrospinning conditions to produce fibers with little to no crossing, highly aligned fiber scaffolds directed neurite outgrowth parallel to the fibers and neurites growing perpendicular to the orientation of the fibers did not occur. The SCs also attached on and grew along the PLLA fibers. In comparison, DRGs grown on fiber specimens that contained crossed fibers grew along the axis of most of the fibers. However, several did also grow along the crossed fibers, and some axons were impeded by the crossed fibers. Using a novel technique to quantify neurite density, it was observed that increasing PLLA fiber density correlated to an increase in neurite density without affecting the length of extending neurites.

2. Materials and methods

2.1. Preparation of aligned PLLA electrospun fibers

PLLA was chosen in this study due to its biocompatibility and biodegradability; 8 wt% PLLA (NatureWorksTM; grade 6201D, Lot #9051-89-2, density: 1.25, weight average MW being 78 kDa and number average MW being 48 kDa, provided by Cargill Dow LLC, Minnetonka, MN) was dissolved in chloroform at room temperature. A modified electrospinning method (Xu *et al* 2004) was used to create aligned PLLA fibers as shown in figure 1. A high-voltage power supply (Gamma High Voltage Research; Ormond Beach, FL) was used to supply the required charge. A multi-speed syringe pump (Braintree Scientific Inc.; Braintree, MA) was placed perpendicularly to the ground. A 5.0 ml glass syringe and

Table 1. Electrospinning parameters varied in the optimization tests.

	Variables	Fixed parameters
Rotation speed of the collector	250 rpm	22 G sharp-tip needle, 4 mL h ⁻¹ , 1 h
	500 rpm	
	1000 rpm	
Needle tip shape and gauge	Flat tip	20 G needle, 1000 rpm, 4 mL h ⁻¹ , 1 h
	Sharp tip	
Insulated needle	Insulated needle	22 G sharp-tip needle, 1000 rpm, 4 mL h ⁻¹ , 1 h
	Flow rate of the syringe pump	22 G sharp-tip needle, 1000 rpm, 1 h
2 mL h ⁻¹		
4 mL h ⁻¹		

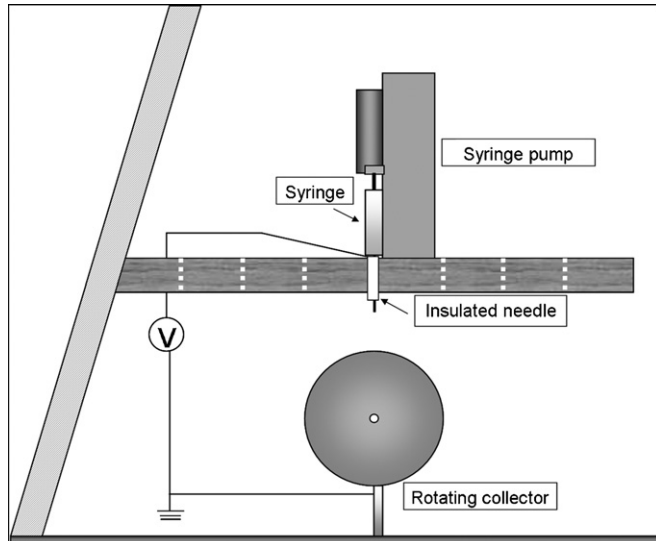


Figure 1. Schematic of the setup to create aligned PLLA fibers by electrospinning using an insulated sharp needle and a rotating disk collector.

one of several needles (20G flat and sharp tip needles with an inner diameter of 0.6 mm, and a 22G sharp-tip needle with an inner diameter of 0.4 mm (Fisher Chemicals; Fair Lawn, NJ)) were used to generate fibers. The needle was connected to the power supply to charge the polymer solution. An aluminum rotating disk (220 mm in diameter with a thickness of 10 mm) attached to a laboratory mixer motor (IKA Works Inc.; Wilmington, NC) was used as the fiber collector. Rotation speeds of 250 rpm (linear distance 172.7 cm min⁻¹), 500 rpm (linear distance 345.4 cm min⁻¹) and 1000 rpm (linear distance 690.8 cm min⁻¹) were used in this study.

The following fixed conditions were used in the experiments: (a) applied voltage: 20 kV, (b) distance between the needle tip and the collector: 5.5 cm, (c) collecting time: 1 h (unless stated otherwise), and (d) a constant room temperature of 26°C and a constant relative humidity of 58%. The fibers were spun onto 12-by-12 mm glass coverslips (Proscitech, Australia) attached on the edge of the rotating disk using a piece of double-sided tape (3M; St Paul, MN).

To determine the optimal electrospinning parameters such as fiber alignment and fiber density for neuronal outgrowth, different electrospinning conditions were tested (table 1). The diameters of the fibers were measured using Scion Image software.

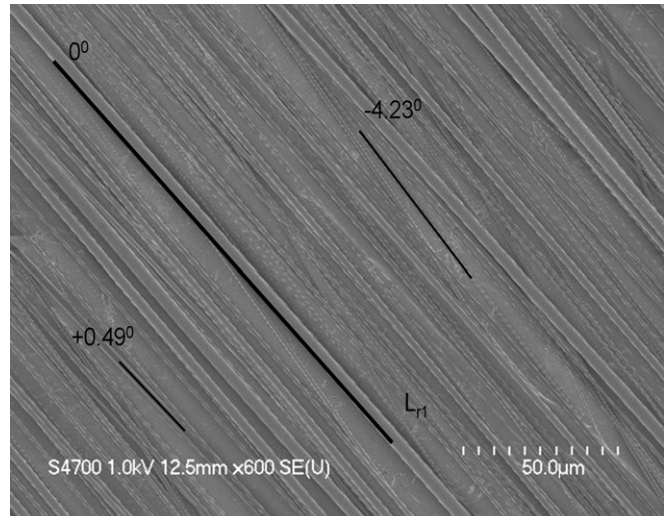


Figure 2. Alignment analysis. The reference line (L_{r1}) represents the uniaxial orientation of most of the fibers. The angle formed between 150 fibers and L_{r1} was measured and averaged.

2.2. Scanning electron microscopy

SEM was conducted using a Hitachi S-4700 field emission scanning electron microscope at an accelerating voltage of 1 kV. Each sample was coated with a 10 nm thick layer of platinum/palladium by a Hummer 6.2 sputter coater (Anatech Ltd. Denver, NC).

2.3. Fiber alignment quantification

To quantify the alignment of fibers, the orientation of 50 fibers on each image (from three images captured from independently fabricated samples) was measured using Scion Image. A reference line was drawn along the central orientation and the angle formed between the line and each fiber was calculated (figure 2). Each angle was placed into a data bin of 2°, so that all angles between 0° and 2° were placed in one bin, all angles between 2° and 4° were placed in another bin, and so on (Biran *et al* 2003). Angles ranged from -90° to 90° with 0° being parallel to the reference line. Thus, 150 fibers were used to generate the fiber alignment graph for each condition.

Fast Fourier transform (FFT) was also used to characterize the alignment of the fibers. The FFT function converts information present in the original image from the 'real' space into the mathematically defined 'frequency' space (Alexander

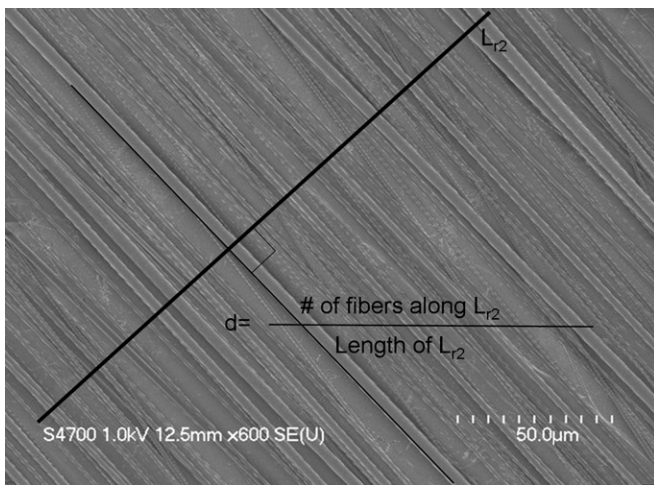


Figure 3. Density measurement. Density (d) is defined as the number of fibers along the reference line (L_{r2}) divided by the length of L_{r2} .

et al 2006). The resulting FFT output image reflects the degree of fiber alignment present in the selected area (Ayres *et al* 2006). A square region of 512×512 pixels on the SEM image was randomly selected and processed for FFT using Scion Image Beta 4.0.3 (Scion Corporation; Frederick, MD).

2.4. Fiber density measurements

A new technique for quantifying fiber density was developed. Six SEM images (two images from three independently fabricated samples) were selected for each condition. As shown in figure 3, a reference line perpendicular to the majority of the fibers was drawn on the SEM image, and the number of fibers along the reference line was counted. The density was averaged, and it is presented as the number of fibers per mm for each condition.

2.5. Creation of crossed fiber specimens and measurement of fiber crossing rate

To evaluate how crossing fibers affect neurite outgrowth, a layer of crossing fibers were electrospun onto aligned fibers. Highly aligned fibers were generated for 10 min using a 22G insulated, sharp-tip needle and using the parameters stated previously (1000 rpm rotation speed for the collection disk and 2 ml h^{-1} syringe pump flow rate). The coverslips were removed from the rotation wheel and reattached after rotating the specimens 45° . Electrospun fibers were placed onto the sample for 3 min using the same parameters specified above. Three batches of crossed fiber specimens were created and imaged using scanning electron microscopy presented in section 2.2. Within each batch, three images were captured and the number of aligned and crossed fibers counted within a selected area (1 mm by 1 mm). The fiber crossing rate equation was used to determine the degree of fiber crossing within the specimen equation (1):

Fiber crossing rate

$$= \text{Number of crossing fibers}/\text{total number of fibers}. \quad (1)$$

2.6. Cell culture

E9 chick DRGs were isolated in accordance with procedures approved by the Institutional Animal Care and Use Committee (IACUC) at Michigan Technological University. The ganglia were divided into halves and placed into a sterile microcentrifuge tube with $200 \mu\text{l}$ of Hank's balanced salt solution (HBSS) (Mediatech, Herndon, VA) and centrifuged at 2000 rpm for 2 min. The supernatant HBSS was removed, and the DRGs were re-suspended into $90 \mu\text{l}$ of neurobasal medium supplemented with L-glutamine, penicillin/streptomycin, and B-27 serum free supplement (Invitrogen, Carlsbad, CA). The suspension was then placed onto crossing fibers and highly aligned PLLA fibers generated with optimal working conditions. To determine how fiber density affected neurite outgrowth, the spinning time was set at 0.5 h and 2 h, which gave significantly different densities. 0.5 h produced low-density fibers and 2 h produced high-density fibers. DRGs were allowed to attach onto three fiber samples (both 0.5 h and 2 h) created from independently fabricated samples that were not coated with any neuronal adherent proteins or serum solutions for approximately 12 h within a tissue culture incubator (37°C , 5% CO_2). Then another 2 ml of neurobasal medium was added with a final concentration of 50 ng ml^{-1} of nerve growth factor (NGF) (Calbiochem, La Jolla, CA). The DRGs were then incubated for 5 days with fresh medium being exchanged every 48 h. Culture experiments were repeated twice to confirm initial results.

Schwann cells (SC) were isolated in accordance with procedures approved by the Institutional Animal Care and Use Committee (IACUC) at Johns Hopkins University. Highly purified cultures were obtained from the sciatic nerves of adult female Fischer-344 rats (Charles River Laboratories) as described previously (Hurtado *et al* 2006) following Morrissey's protocol (Morrissey *et al* 1991). Dissociated SCs were cultured on poly-L-lysine coated tissue culture dishes in D10 medium (DMEM (Invitrogen, Carlsbad, CA) with 10% fetal bovine serum (Hyclone, Logan, UT) and 0.1% Gentamicin (Invitrogen)) supplemented with the mitogens bovine pituitary extract (2 mg ml^{-1}), forskolin (0.8 g ml^{-1}), and heregulin (2.5 nM). The solution of heregulin is a previously described (Levi *et al* 1995) modification of the original protocol (Morrissey *et al* 1991). To determine the purity of the SCs used, samples of the harvested cells were plated onto culture dishes, cultured for 3 h, stained for S100, and then coverslipped with Citifluor (UKC Chemical Laboratory, Canterbury, UK) with $100 \mu\text{m}$ Hoechst nuclear dye (Sigma, St Louis, MO) to compare numbers of S100-positive cells with Hoechst-labeled cells. The purity of the SCs used was 95–98%. At early passage, SCs were transduced overnight with a lentiviral vector encoding green fluorescent protein (GFP) (Naldini *et al* 1996) at a multiplicity of infection of 30. The production of the lentiviral vectors has been previously described (Blits *et al* 2005). GFP expression was controlled by the cytomegalovirus promoter and enhanced with the woodchuck post-transcriptional regulatory element (Loeb *et al* 1999). The transduction efficiency in the SC cultures was >99%. The transduced SCs were further cultured until passage 4 and then collected (Morrissey *et al*

1991) for plating onto three high- and three low-density fiber samples with a cell density of 150 000 cells/100 μl D-10 medium. SCs were allowed to attach onto three fiber samples of independently fabricated samples for approximately 12 h within a tissue culture incubator (37°C , 5% CO₂), after which another 2 ml of D-10 medium was added. The SCs were then incubated within the fiber scaffolds for 2 days. Experiments were repeated to confirm initial results ($N = 2$).

2.7. Immunocytochemistry

After 5 days in culture, DRGs were fixed in a PBS (10 mM phosphate, 150 mM sodium chloride) solution containing 4% (wt/volume) paraformaldehyde (Sigma-Aldrich; St Louis, MO) for 30 min. DRGs were washed three times with PBS, and then blocked with a PBS solution containing 1% normal goat serum (Chemicon, Temecula, CA), 2% non-fat dry milk (TVC Inc.; Brevard, NC) and 0.05% triton X-100 (EMD Chemicals, Gibbstown, NJ) for 15 min. After washing the specimens three times with PBS, DRGs were incubated (37°C , 5% CO₂) with rabbit anti-neurofilament primary antibody (1:200 dilution, Chemicon, Temecula, CA) for 1 h, washed three times with PBS; specimens were incubated with an Alexa Fluor 488 goat anti-rabbit secondary antibody (Invitrogen; Carlsbad, CA) for another hour, and washed three times with PBS. The SCs were washed three times with PBS before fluorescence microscopy. Both DRGs and SCs were imaged using a Zeiss Axiovert 200 M microscope equipped with an AxioCam fluorescence camera. Zeiss filter set 10 was used where fluorescent dyes with excitation wavelengths between 450 and 490 nm and emission wavelengths between 515 and 565 nm are analyzed. Using this filter set, autofluorescence from the electrospun fibers was not observed.

2.8. Quantification of the density of neurite outgrowth

DRGs were placed onto three independently fabricated fiber samples for each fiber condition (low density and high density) in two separate instances ($N = 2$). When the neurite outgrowth was longer than 1.5 times the DRG explant diameter, the DRG was considered vital (Kim *et al* 2005) and was selected for subsequent analysis. Eight DRG explants were selected from the low-density fibers (electrospun for 0.5 h), and seven from the high-density fibers (electrospun for 2 h). To distinguish neurite extension from the background of the fluorescent images, procedures were used similar to those published elsewhere (Bilsland *et al* 1999, Deister and Schmidt 2006). The micrographs were processed using a processing technique that involved using Adobe® Photoshop CS3. DRGs were removed from the images, as only neurite outgrowth was targeted for measurement. Neurite density was measured by finding the percentage of fluorescence in the extension area after neurofilament staining. Images were imported into Scion Image software, and thresholding was used to identify the fluorescent pixels. Images were then converted to binary images composed solely of white and black pixels, black indicating fluorescence and white indicating the background. Using the measure function within Scion Image, the total area (A_0 ; includes DRG and its neurites), the average gray value of

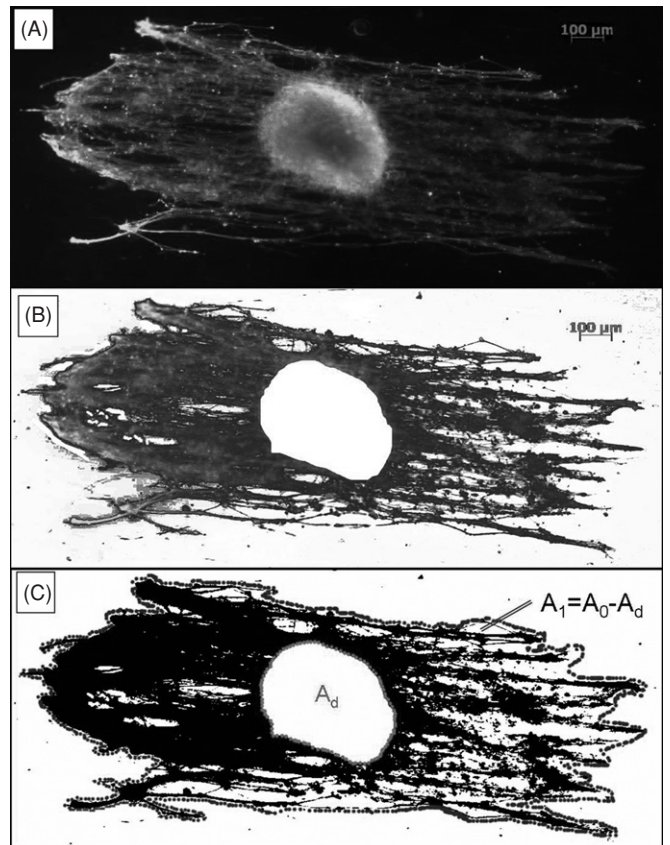


Figure 4. Diagram of axonal density measurement. (A) Original neurofilament-stained image. (B) Photoshop processed image. (C) Measured binary image.

the total area (A_0) and the area of the removed DRG (A_d) were determined. The gray value of a black pixel is 255 and the gray value of a white pixel is 0. The number of black pixels (x_1) in the total area can be determined using equation (2). The neurite outgrowth area (A_1) was obtained by subtracting the area of the DRG (A_d) from the total area (A_0), as shown in equation (3). The percentage of black pixels (% fluorescence), which indicates the density of neurite outgrowth, can be determined by taking the number of black pixels (x_1) divided into the area of neurite outgrowth (A_1) (equation (4)). The original image, processed image and the measured binary image are shown in figures 4(A), (B) and (C), respectively:

$$x_1 = \frac{\mu_0 A_0}{255} \quad (2)$$

$$A_1 = A_0 - A_d \quad (3)$$

$$\% \text{ fluorescence} = \frac{x_1}{A_1} \times 100. \quad (4)$$

2.9. Quantification of the length of neurite outgrowth

The same DRGs mentioned above were selected for neurite outgrowth measurement. Ten of the longest neurites from each side of the DRG explants were measured and averaged to quantify neurite length under different density conditions. The perimeter of each DRG was marked and the length of the neurite was measured from the tip of the neurite to the marked perimeter using Scion Image.

2.10. Statistical analysis

Statistical analyses were performed using JMP IN software (Release 5.1.2; SAS; Cary, NC). A one-way ANOVA was run first to determine statistical differences between groups in fiber density ($N = 6$), neurite density measurement ($N = 8$ for low density and $N = 7$ for high density) and neurite length ($N = 160$ for low density and $N = 140$ for high density). For those that showed differences in ANOVA, *post-hoc* Tukey–Kramer HSD tests were used to compare all pairs individually. The Brown–Forsythe test was run to determine statistical differences in fiber alignment ($N = 150$). A value of $P < 0.05$ was considered to be statistically significant.

3. Results

3.1. The effect of rotation speed

The effect of rotation speed of the collector was studied at speeds of 250 rpm, 500 rpm and 1000 rpm. A 22 gauge, sharp-tip needle with an inner diameter of 0.4 mm was used with a flow rate of 4 ml h^{-1} . SEM images (figures 5(A)–(C)), FFT output images (figures 5(D)–(F)) and the angle difference measurements (figures 5(G)–(I)) demonstrate the alignment of the fibers. FFT images were taken from 512×512 pixel selections of the original SEM images and generated an output image containing pixels with a symmetrical shape. The narrower area of the center parts in FFT output images indicates better fiber alignment. Figure 5 shows improved alignment with increased rotation speed. Figures 5(F), (I) show that the best alignment was obtained with a rotation speed of 1000 rpm. Fiber diameters varied between 1.2 and $1.6 \mu\text{m}$ at a rotation speed of 1000 rpm.

Even though highly aligned fibers were successfully fabricated, the efficiency of electrospinning/collection, related to the density of the fibers, was very low while using a 22G sharp-tip needle, as shown in figure 5(J). Therefore, it was hypothesized that a needle with a bigger diameter or with a flat tip may give higher efficiency.

3.2. The effect of needle size and tip shape

20G needles (an inner diameter of 0.6 mm) with a sharp-tip and a flat-tip were used to fabricate the fibers. The corresponding SEM images and FFT output images are shown in figures 6(A), (B) and (C), (D), respectively. Figures 6(E) and (F) show the angle difference measurements for the flat and sharp tip needles, respectively. The rotation speed was fixed at 1000 rpm and other conditions were unchanged. Figures 6(D) and (F) demonstrate that a 20G sharp-tip needle generated fibers that were more aligned than those fibers generated by a 20G flat-tip needle, shown in figures 6(C) and (E), but still not as aligned as the fibers generated by a 22G sharp needle ($*P < 0.05$). However, a 20G needle (bigger diameter) produced more fibers (improved efficiency) than using a 22G needle (figure 6(G)). Since the 22G needle produced highly aligned fiber species, other needle types were not investigated.

3.3. The effect of a modified needle on the efficiency

Because fibers are being developed for neural tissue engineering applications, the alignment of fibers is critical for directing neurite outgrowth in a particular direction optimally. Our results suggest that if the electrospinning efficiency can be improved, a 22G sharp-tip needle would be the best choice to generate the highest degree of alignment. Thus we hypothesized that increasing the intensity of the electric field on the tip of the needle may increase the efficiency of electrospinning. Based on this hypothesis, a piece of tubing (Masterflex®, Tygon®, Fisher Scientific, Pittsburgh, PA) was used to insulate the 22G needle body, leaving only the needle tip exposed to the electric field. A SEM image, a FFT image and angle difference analysis (figures 7(A)–(C)) show that the fibers were still highly aligned; figure 7(D) reveals that the density of the fibers generated by the modified 22G needle was much higher than that of the 22G uninsulated needle ($*P < 0.05$).

3.4. The effect of flow rate

A 22G insulated, sharp-tip needle was used at flow rates of 2 ml h^{-1} and 4 ml h^{-1} respectively in order to study the effect of the flow rate on fiber alignment. Figures 8(A)–(C) contain a SEM image, a FFT image and angle difference analysis. The results show that there is no significant difference with a flow rate of 2 ml h^{-1} or 4 ml h^{-1} either on alignment (figures 8(A)–(C)) or fiber density (figure 8(D)). However, with the flow rate of 4 ml h^{-1} , more residue was generated because the solvent evaporated before the fibers had formed completely. Therefore, a flow rate of 2 ml h^{-1} was used for all other studies. Upon optimization of electrospinning parameters, fiber scaffolds were created where 84%, 96% and 99% of the fibers deviated no more than $\pm 2^\circ$, $\pm 5^\circ$ or $\pm 10^\circ$ from a reference line parallel to the aligned fibers. Fiber diameters varied between 1.2 and $1.6 \mu\text{m}$ under the optimal conditions.

3.5. The effect of crossing fibers on neurite outgrowth

Embryonic E9 chick DRGs were cultured on the coverslips containing highly aligned fibers described above (figure 8(A)) and crossing fibers with a crossing rate of 28%. The average crossed angle was 45° to the previous aligned fibers as shown in figure 9(A). Figure 9(B) clearly demonstrates that neurite orientation was diverted away from the axis of alignment and in some cases restricted by the crossing fibers.

3.6. The effect of fiber density on neurite outgrowth

Embryonic E9 chicken DRGs were selected on low-density (0.5 h) and high-density (2 h) fibers to investigate the effect of the PLLA fiber density on neurite outgrowth. After 5 days of incubation, the DRGs were stained for neurofilaments. Figures 10(A) and (B) show SEM images of the fibers and figures 10(C) and (D) show fluorescent images of neurofilament-stained neurites. The density of fibers, axon density and outgrowth length are shown in figures 10(E), (F)

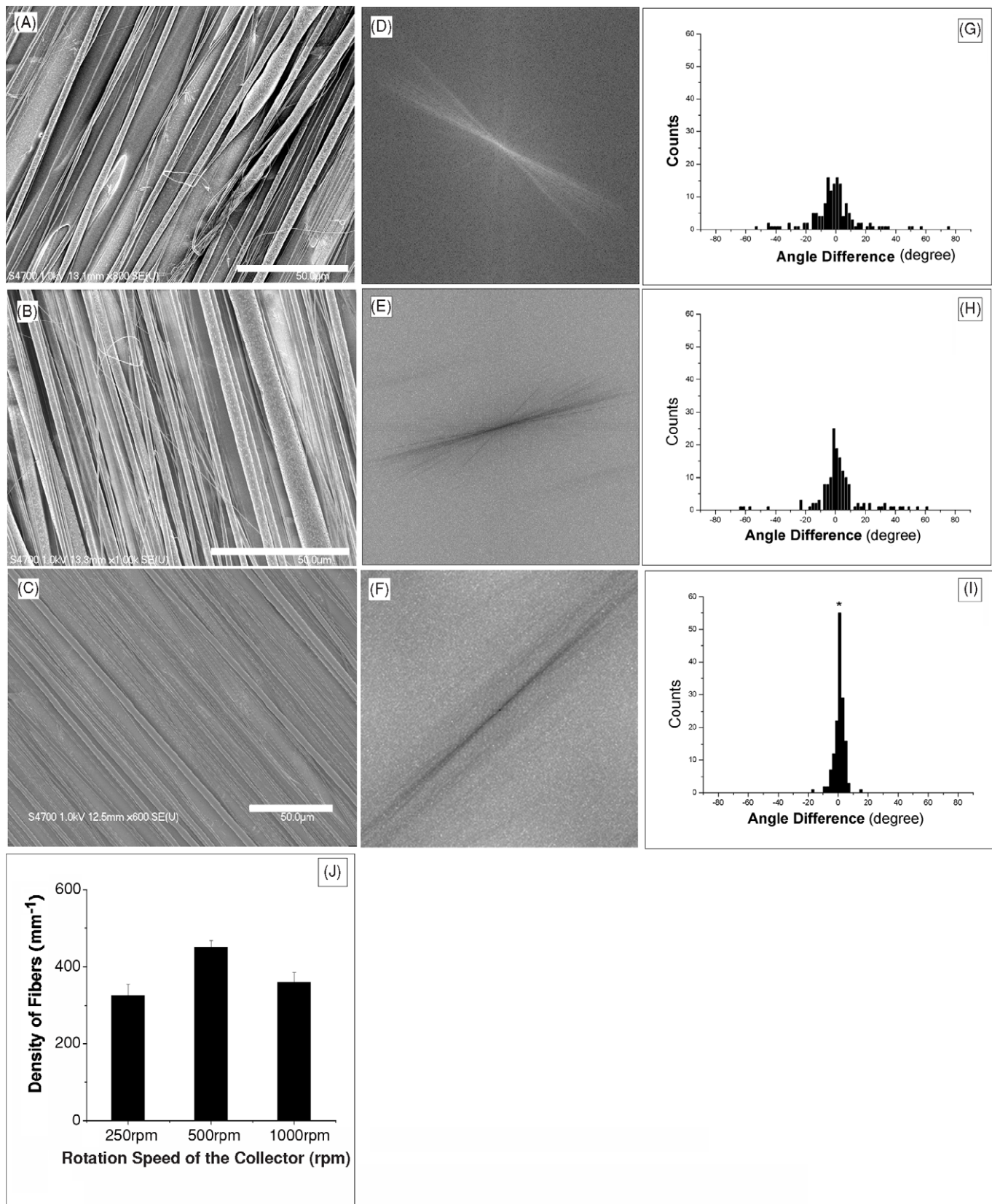


Figure 5. Alignment and density of PLLA fibers using different collection disk rotation speeds. (A–C) SEM images of fibers collected with a rotation speed of 250 rpm (A), 500 rpm (B), and 1000 rpm (C) (scale bar = 50 μm). (D)–(F) FFT images from 512 × 512 pixel selection from images (A)–(C), respectively. The center area depicts the alignment of the fibers. The narrower areas represent the most highly aligned fiber specimens. (G)–(I) Histograms of angle difference showing the alignment of fibers in (A)–(C), respectively. The best fiber alignment was obtained when using a rotation speed of 1000 rpm as depicted in panel I (* $P < 0.001$). (J) Plot of the fiber density collected under different rotation speeds.

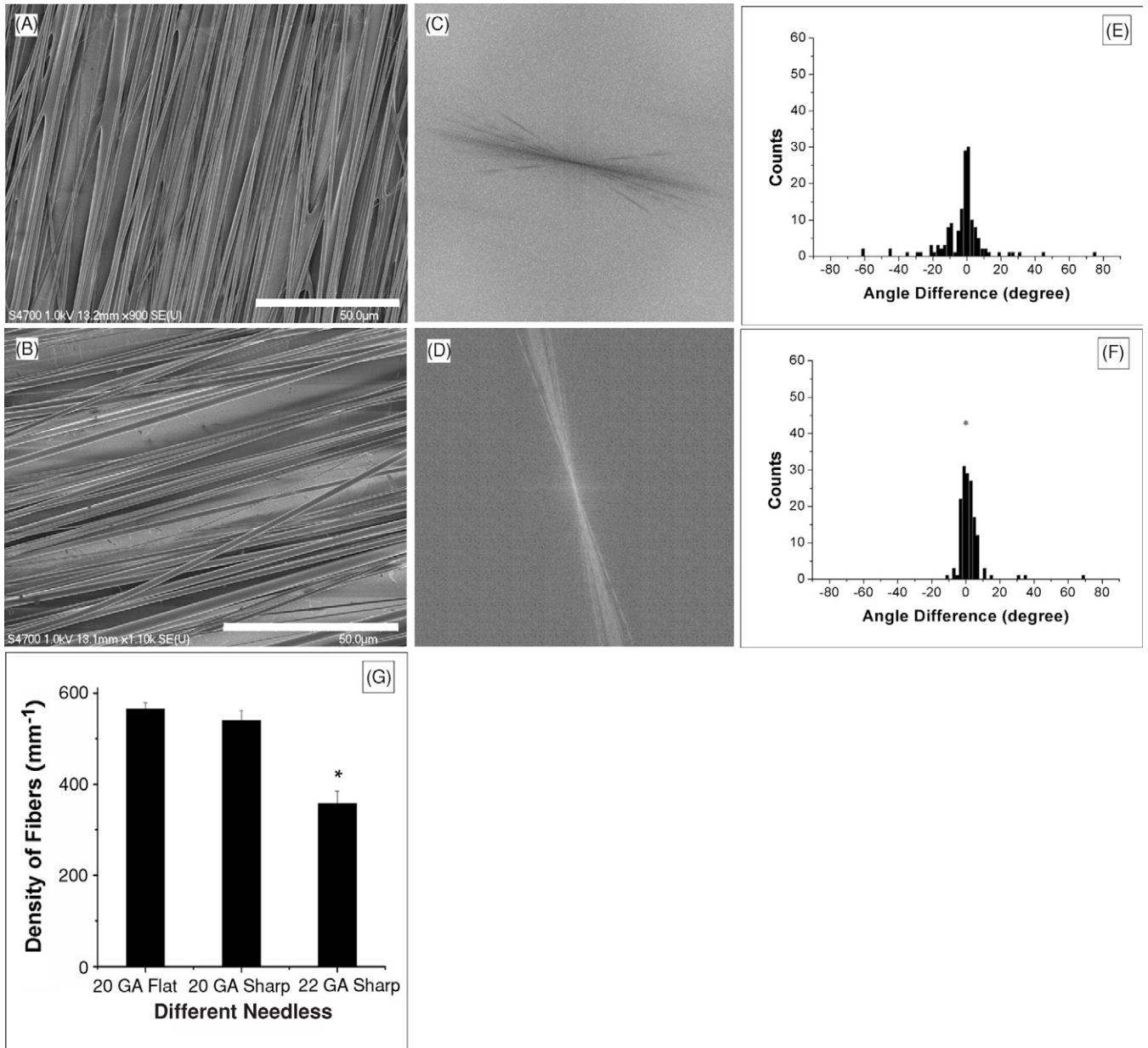


Figure 6. Effects of needle size and tip shape on fiber alignment and density. SEM images of fibers produced using a 20G, flat-tip (A) and sharp-tip (B) needle (scale bar = 50 μm). (C) and (D) FFT images from 512 \times 512 pixel selection from images of (A) and (B), respectively. (E) and (F) represent the fiber alignment analyses. The best fiber alignment was obtained with a sharp 20G needle as compared to the flat 20G one (* $P < 0.001$). (G) Density plot showing that the 20G needle is more efficient than the 22G needle (* $P < 0.05$).

and (G), respectively. The results suggest that highly aligned fibers guide neurite outgrowth in a directed manner. The density of neurites (figure 9(F)) increased with increasing fiber density, $65\% \pm 14$ of the fluorescence for the low density and $83\% \pm 6$ for the high density (* $P < 0.05$). The length of the neurite outgrowth for 0.5 h was $1210 \pm 345 \mu\text{m}$ and for 2 h was $1054 \pm 249 \mu\text{m}$ (mean \pm standard deviation). Statistical analysis showed no significant difference in neurite length.

3.7. Schwann cells on PLLA fibers

Schwann cells display a typical bipolar, swirling morphology when cultured on a poly-L-lysine coated dish (figure 11(A)).

Schwann cell growth on a dish is not directed. Within the fiber cultures, SCs grew in a directed manner along the fibers in both the low (figure 11(B)) and high (figure 11(C)) density samples. More Schwann cells were seen in the higher density fiber sample.

4. Discussion

4.1. Alignment of electrospun fiber species

Aligned, electrospun fibers have been fabricated (Teo *et al* 2005, Pan *et al* 2006) for drug delivery (Chew *et al* 2005) or tissue engineering applications (Baker *et al* 2008, Chew *et al* 2008, Choi *et al* 2008). Recently, electrospun fiber

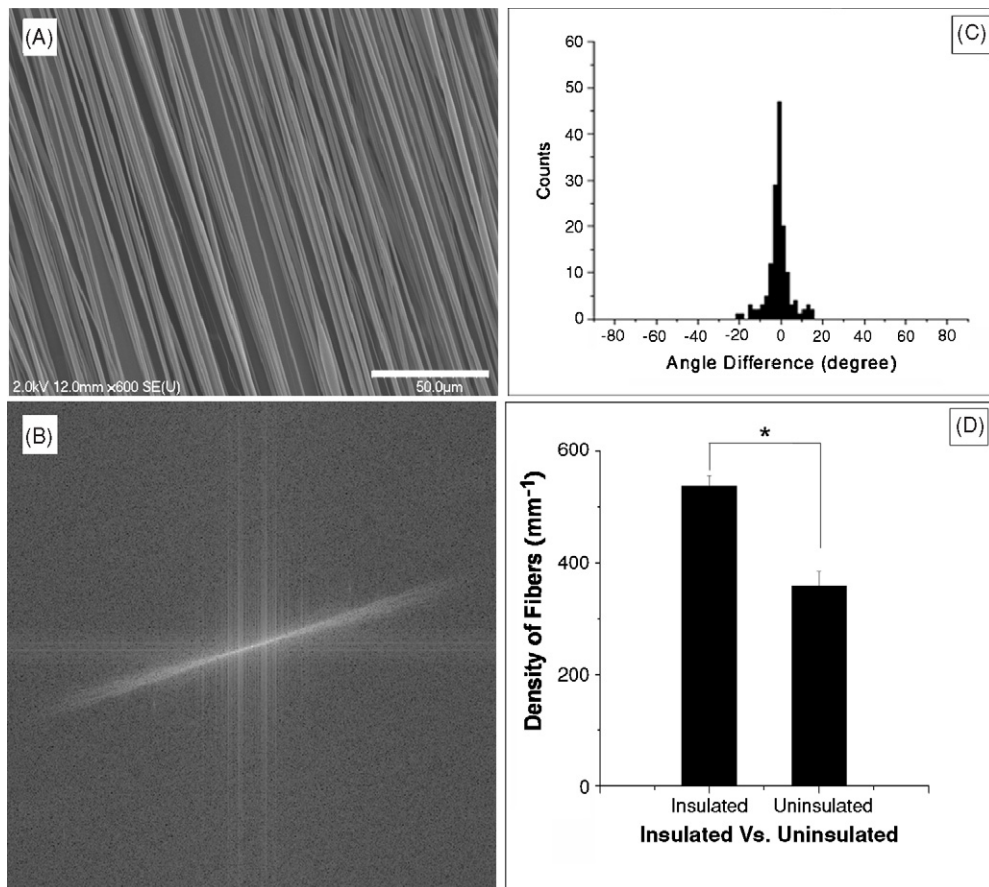


Figure 7. Effects of modified needle on fiber density which is related to electrospinning efficiency. (A) SEM image of the fibers produced with an insulated needle at the flow rate of 4 ml h^{-1} for 1 h. (B) FFT image from 512×512 pixel selection from image (A). (C) Fiber alignment using insulation. (D) Density plot reveals that the density of fibers (A) is much higher than that using an uninsulated needle (compared to figure 5(C)) ($*P < 0.05$). Scale bar = $50 \mu\text{m}$.

structures have shown great promise in directing neurite outgrowth in a particular direction in both *in vitro* (Corey *et al* 2007, 2008, Schnell *et al* 2007, Kim *et al* 2008) and within *in vivo* models (Chew *et al* 2007, Kim *et al* 2008). While these studies suggest that fiber alignment is important in directing neurite outgrowth, further optimization of fiber characteristics may be required. For example, optimally aligned fiber scaffolds that minimize fiber crossing may better direct neurite outgrowth, potentially improving functional recovery and/or decreasing the amount of time that a functional deficit exists.

Since previous observations in our laboratory and by others (Corey *et al* 2007, Kim *et al* 2008) show that randomly oriented fibers have the potential to impede axonal outgrowth, the goal of this study was to produce highly aligned electrospun scaffolds. In the present study, electrospinning conditions were investigated in order to produce highly aligned fibers from an 8 wt% PLLA solution in chloroform. While maintaining the same voltage, distance between the needle tip and the collector, and the same room temperature and humidity conditions, four electrospinning parameters were varied: the collection disk rotation speed, the inner diameter size of the needle, the shape of the needle tip and the syringe pump flow rate. After a series of optimization tests, it was determined that a collection disk rotation speed of 1000 rpm, a 22G sharp

needle and a syringe pump flow rate of 2 ml h^{-1} produced highly aligned fiber scaffolds. Furthermore, when chick DRG explants were placed onto the scaffolds, increased neurite density was seen when explants were cultured on high-density aligned fiber substrates. Schwann cells placed onto the aligned fiber scaffolds exhibited an extended or stretched morphology as seen in other studies (Chew *et al* 2008).

This work shows that at 1000 rpm, the most aligned PLLA electrospun fibers were fabricated. The reason behind this result may be due to the fact that a high collection disk rotation rate stretches the fibers into an aligned and uniform orientation without fiber breakage. At lower rates (250 and 500 rpm) the alignment was lower, and when the rotation speed was higher than 1000 rpm, the collection efficiency decreased (data not shown) because fibers were diverted away from the collecting disc by air flow from the rotation of the disk. Therefore, fewer fibers were attached to the collector.

The process of electrospinning has been described previously (Fong *et al* 1999, Deizel *et al* 2001, Huang *et al* 2003) and has revealed that when an electric field is applied to a needle, the polymer fluid forms a conical shape at the tip of the capillary known as the Taylor cone (Fong and Reneker 1999). The driving force, which is related to the intensity of the electric field, opposes the surface tension

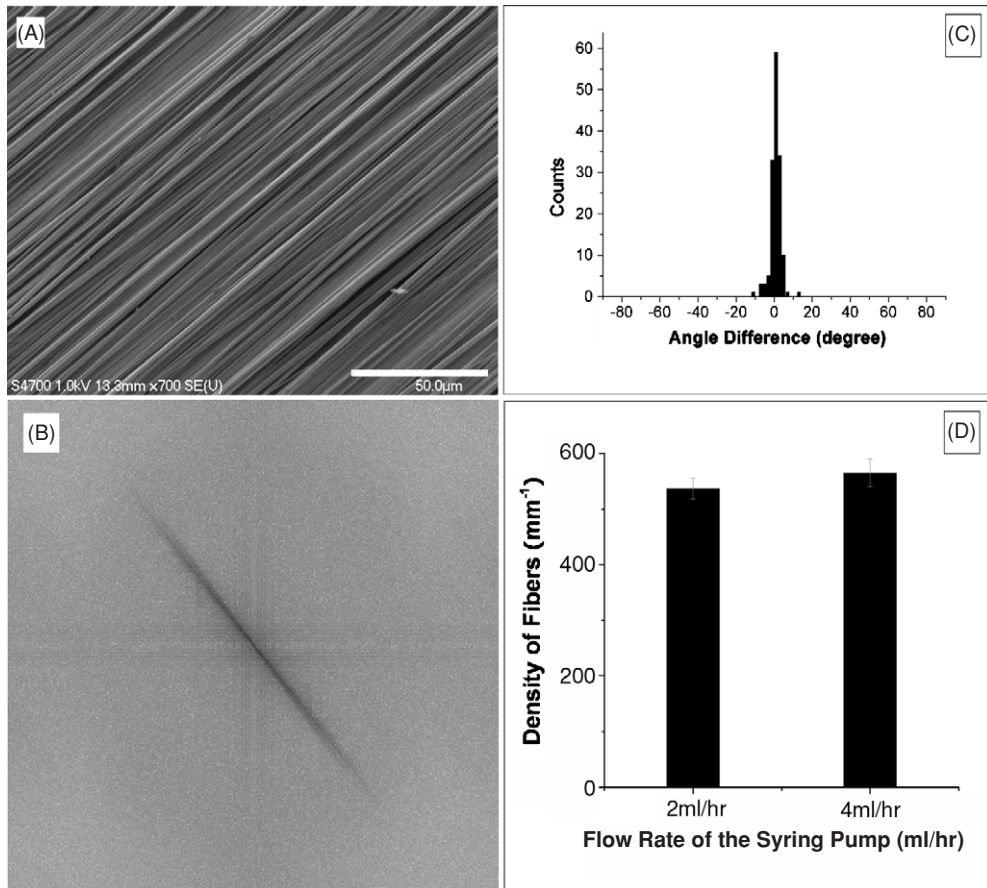


Figure 8. Alignment and density of the fibers generated by a 22G insulated, sharp-tip needle at a flow rate of 2 ml h^{-1} . (A) SEM image of the fibers produced with a flow rate of 2 ml h^{-1} . (B) FFT image from 512×512 pixel selection from image (A). (C) Alignment of sample A. (D) Density plot. Neither the alignment (A)–(C) nor density (D) is significantly different when different flow rates were applied. Scale bar = $50 \mu\text{m}$.

of the polymer fluid. Beyond a critical point, the Taylor cone is unstable and a charged polymer jet ejects out and is deposited onto a grounded collector. As the solvent evaporates, the jet solidifies to form nano or microfibers (Rutledge and Fridrikh 2007). Since electrospinning highly aligned fibers is an inherently difficult process that depends on several factors, manipulation and characterization of factors to create highly aligned fiber species provides a useful tool for creating such scaffolds.

4.2. Needle insulation improves electrospinning efficiency

The 22G needle allowed for the creation of highly aligned fiber species in comparison to when the 20G needle was used, but the electrospinning efficiency (the number of fibers collected over time) was lessened. The electrospinning efficiency was also enhanced using a novel needle insulation technique that has not been published before. It is postulated that when the entire needle is charged, without insulation, the electric field surrounds the needle. Electrical forces around the needle pull fibers away from the collection disk. Surrounding the needle with insulation dampens the electrical field around the needle, and thus more fibers are deposited onto the collection disk.

4.3. Culturing neurons on highly aligned and crossed fiber species and assessing directed neurite outgrowth

Culture of primary neuronal cells on aligned fibers has improved directed outgrowth of neurites (Corey *et al* 2007, 2008, Kim *et al* 2008). From these recent studies, fiber alignment was assessed using the fast Fourier transform (FFT) followed by computer analysis or by manually measuring the angle difference of each fiber from a reference line parallel to the aligned fibers. Although more aligned than random or intermediate aligned fibers, fibers still crossed as shown in the SEM images of these studies. The inclusion of crossed fibers within samples is significant. To better understand how extending neurites might alter neurite outgrowth, a crossed fiber scaffold was created. Culturing DRGs on the crossed fiber specimens shows that highly aligned fiber species are very significant because the crossing fibers changed the neurite's orientation and even stopped directing neurite outgrowth in some instances.

In this study, FFT analysis was used in concert with manual determination of fiber alignment. Fibers generated using our optimized electrospinning parameters produced fiber scaffolds where 84%, 96% and 99% of the fibers deviated no more than $\pm 2^\circ$, $\pm 5^\circ$ or $\pm 10^\circ$ from a reference line parallel to the aligned fibers, respectively. Direct comparison of fiber

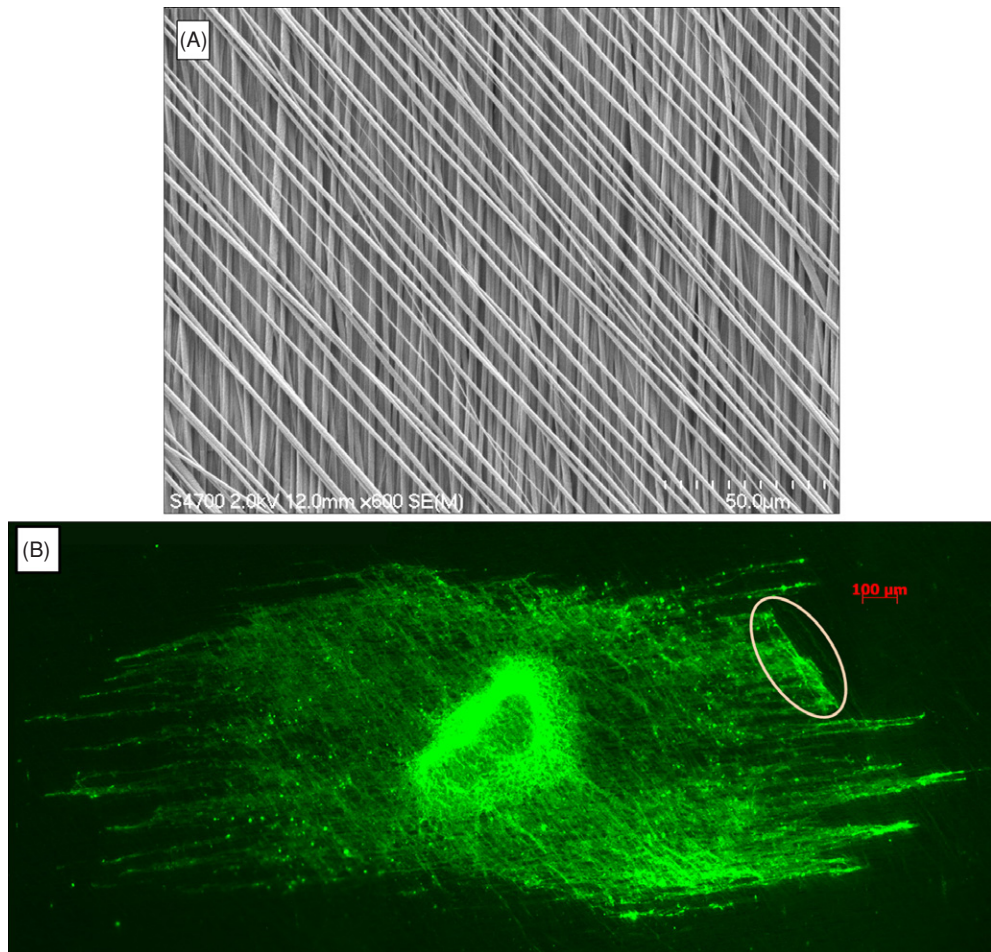


Figure 9. Effects of crossing fibers on neurite outgrowth. (A) SEM image of crossing fibers with a crossing angle of 45°. 28% of the total fibers were crossing fibers. Scale bar = 50 μm . (B) Neurofilament-stained image of DRGs cultured for 5 days on crossing fiber scaffolds. Neurites extended along the crossed fibers and in some instances were impeded by the crossing fibers (circled area) Scale bar = 100 μm .

alignment from our study with others (Corey *et al* 2007, 2008) is difficult since alignment in these studies is computed from FFT images and full width–half max analysis (FWHM). While FWHM analysis provided insight into the aligned character of fiber scaffolds, additional alignment characterization using other approaches provide clearer characterization of fiber alignment.

Corresponding neurite outgrowth from DRGs was less aligned than the fiber alignment (Corey *et al* 2007) whereas similar when dissociated primary neurons were used (Corey *et al* 2008). Our culture data also show directed neurite outgrowth from our DRG explants, but neurite outgrowth was not as aligned as fiber alignment. This is likely due to the fibers separating from the glass coverslip during cell staining and not because of the lack of fiber alignment in our created scaffolds. As the ultimate goal is to apply the aligned fiber substrates into a three-dimensional model for *in vivo* study, our laboratory is developing strategies to secure aligned fibers in place for *in vitro* analysis and for incorporation into a three-dimensional nerve bridge. Strategies using polymer films placed onto coverslips prior to electrospinning (Chew *et al* 2007) is one method being pursued to stabilize fiber alignment (Corey *et al* 2008). However, the use of films may shield

fibers from the grounded collecting disk, requiring additional manipulation of electrospinning parameters to achieve highly aligned fiber specimens.

4.4. Increased polymer fiber density correlates to higher neurite density but unchanged average neurite length

None of these recent studies have examined how fiber density affects neurite outgrowth. Our laboratory has developed a rational technique for determining fiber density where a line is drawn perpendicular to the axis of fiber alignment. The number of fibers on this line is counted to yield the number of fibers per millimeter (figure 3). Additionally, the neurite density was computed using a technique similar to that presented elsewhere (Bilsland *et al* 1999, Deister and Schmidt 2006). In our method, black pixels (figure 4(C)), which represented neurite outgrowth, were divided by the total number of pixels in the whole neurite area (A_1) to calculate the fluorescent percentage as the neurite density. Others have used the area of the actual neurite coverage divided by the entire neurite coverage area to calculate neurite density (Shah *et al* 2004). Here, instead of using the stained area to indicate the neurite density, the fluorescent pixels within

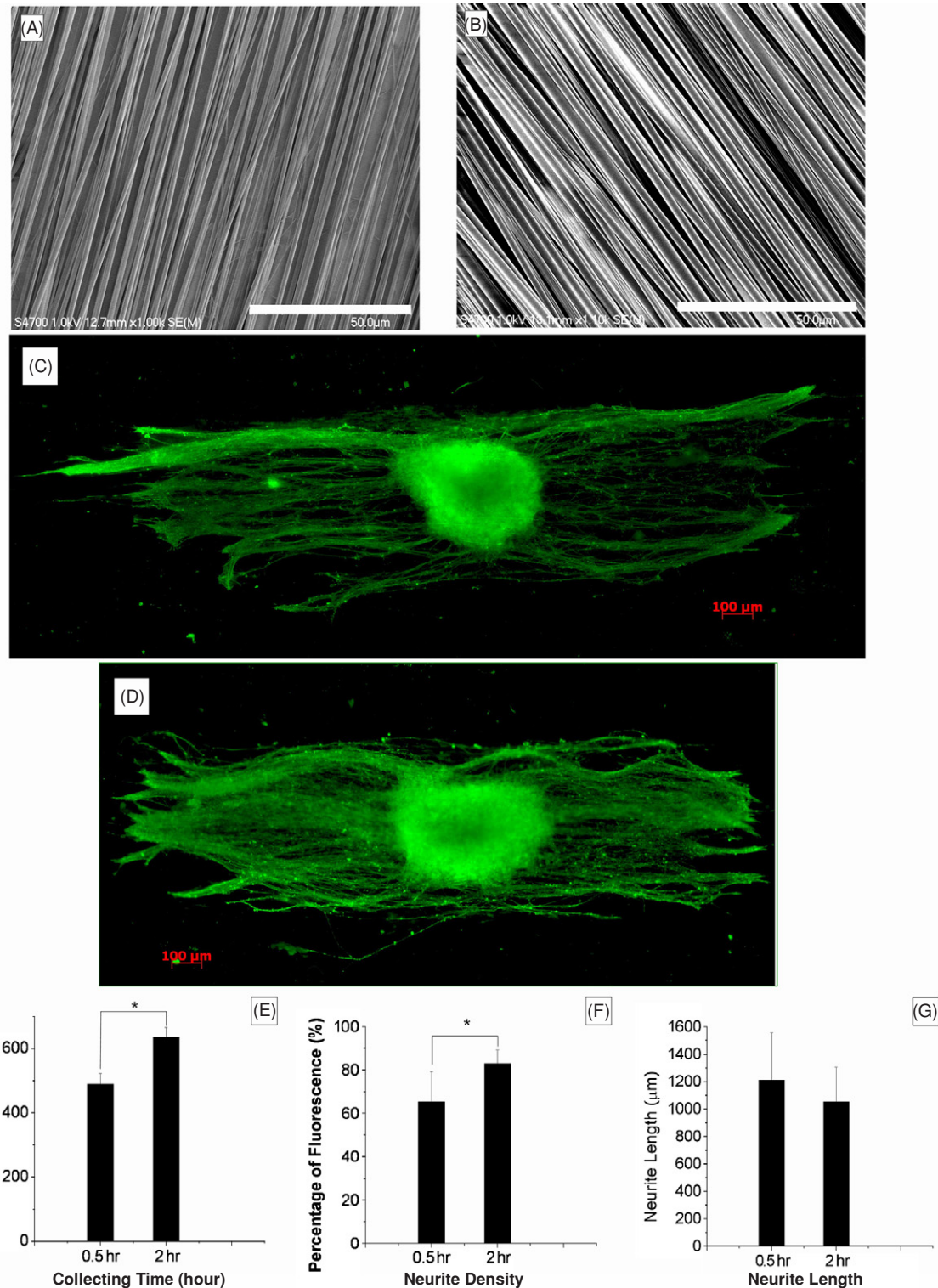


Figure 10. Effects of fiber density on neurite outgrowth. (A) and (B) SEM images of fibers electrospun at 0.5 h and 2 h respectively. (C) and (D) Neurofilament- stained images after DRG were grown on the fibers for 5 days. (E) and (F) The density of the fibers and the density of axonal outgrowth on each fiber condition ($P < 0.05$), which showed that the density of neurite outgrowth was proportional to the density of the scaffold. (G) The neurite length on each fiber condition which was not significantly different.

images containing neurites were detected automatically using Scion Image, creating a more accurate representation of neurite density than other techniques.

Using these novel techniques, it was determined that neurite density increased with fiber density. Thus, this

suggests that more fibers within an area of scaffold lead to more neurites interacting with the scaffold. When thinking of the electrospun fibers, the fibers can be thought of as being a ridge, while the space between fibers can be thought of as being a groove. The dimensions of grooves (space

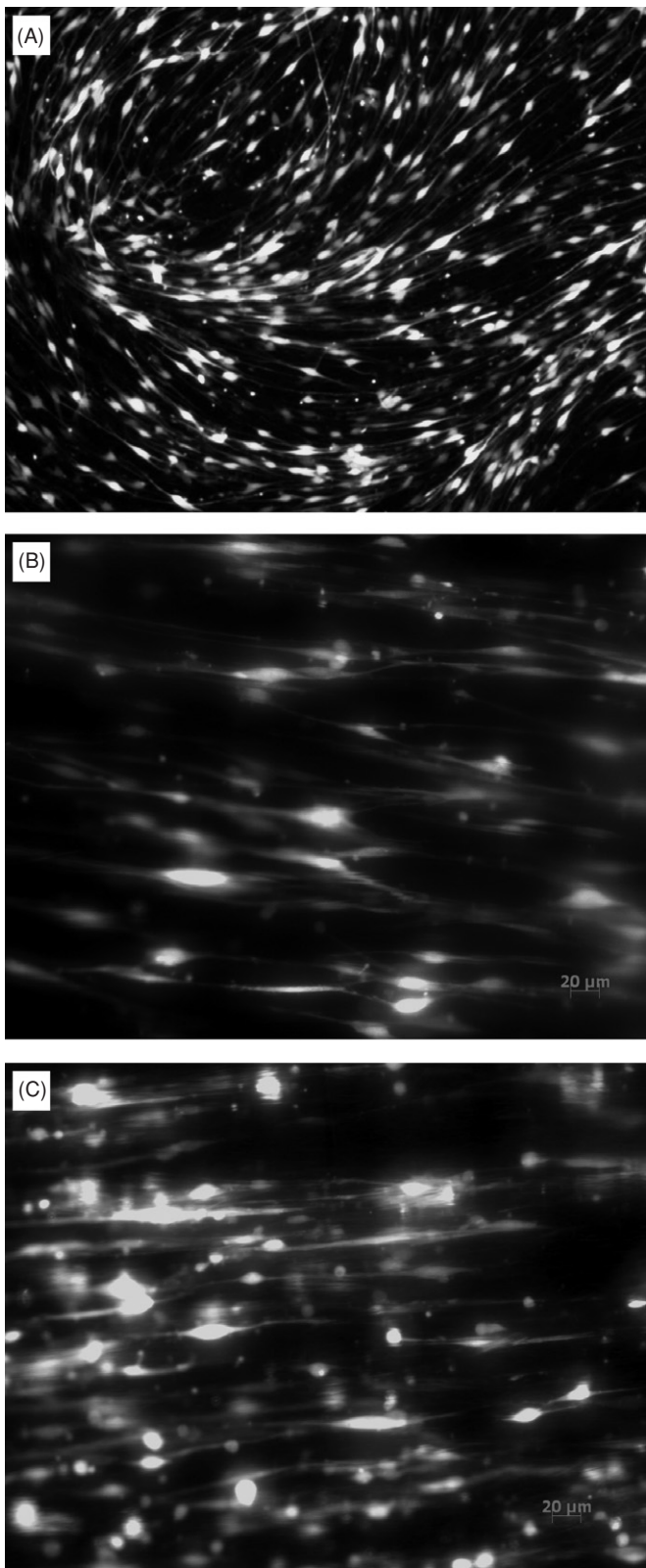


Figure 11. Schwann cell morphology on different substrates.
 (A) Fluorescent image of SCs grown on a poly-L-lysine coated dish, which displays the bipolar, swirling, but undirected growth of SCs.
 (B) and (C) Fluorescent images of Schwann cells cultured on low- and high-density fibers respectively for 2 days. On the fibers, Schwann cells grew along the fibers in a directed manner. Scale bar = 20 μm .

between fibers) and ridges (diameter of fibers) are critical parameters that should be optimized to efficiently guide the greatest population of neurites as possible. The dimensions of grooves and ridges have been previously studied in terms of directing cellular outgrowth. Manwaring *et al* studied the guidance of meningeal cells on imprinted grooved substrates where grooves varied from 10 nm to 940 nm (Manwaring *et al* 2004). Their results show that the alignment of meningeal cells increased with increasing surface roughness in which the best alignment was found when the depth of grooves was 940 nm. Similarly, other studies have observed axonal outgrowth along larger filament diameters ranging from 5 to 500 μm , the most aligned and robust axonal outgrowth was achieved using the 5 μm diameter (Wen *et al* 2006). In another study, when the guidance diameter was less than 1 μm , axons grew or crossed over ridges rather than staying within the grooves (Johansson *et al* 2006).

Fiber diameters within this study were larger than those in other studies (Corey *et al* 2007, 2008, Kim *et al* 2008). Neurite crossing seen within these studies involving *in vitro* DRG cultures may be attributed to smaller fiber diameters or the presence of Schwann cells (Corey *et al* 2007, Kim *et al* 2008). However, when cultured without other cell types, neurites from motor and sensory neurons primarily grew parallel to fiber alignment, but crossing of neurites onto other fibers appeared to occur (Corey *et al* 2008). Taken together, these results suggest that the optimal fiber diameter to direct embryonic chick DRG neurite outgrowth may be between 1 and 5 μm . In addition to fiber density affecting the amount of neurite outgrowth, our Schwann cell culturing results revealed a similar trend in that higher fiber densities supported more Schwann cell attachment.

While neurite density was affected by the number of fibers present, the average neurite length was not significantly different between the two different fiber density scaffolds. The average neurite length mean on the low-density fibers was slightly higher than the average neurite length mean on the high-density fibers. In the 2 h electrospinning situation, fiber structures were layered. However, neurites did have a tendency to follow polymer fibers below the layer closest to the DRG (data not shown). Thus, neurite outgrowth in thicker fiber specimens may facilitate growth through different planes of fibers instead of down the axis of the scaffold. This may be one explanation for the neurite outgrowth on the high-density scaffold being slightly shorter than neurites on the lower density scaffold. However, further morphological study is necessary to ascertain the precise mechanism by which neurites use the polymer fibers to direct their outgrowth.

4.5. Important parameters to consider when designing aligned, electrospun fibers for nerve regeneration application

Therefore, to produce electrospun scaffolds for nerve regeneration applications, the following geometric factors should be considered when developing an implantable scaffold: fiber alignment, fiber density and fiber diameter. While this study shows that very highly aligned fibers direct

neurite outgrowth, the spacing between fibers (width of groove) which is related to fiber density also influences the amount of axonal attachment. The diameter of regenerating axons in relation to the fiber diameter is another aspect to consider. In vertebrates, there is a large variation in the size of axons, ranging between less than 1 μm and up to 50 μm (Rydmark 1981, Matthews 1998). In the present study, the fiber diameter was on the same scale as the neurites. Based on these results, the diameter of the fiber scaffold should be related to the axonal diameter. Fiber diameters one- to three-fold greater than axonal diameters might be of sufficient diameter for nerve scaffold design.

5. Conclusion

According to these results, highly aligned PLLA fibers can be fabricated by carefully manipulating electrospinning parameters. These fibers directed the outgrowth of neurites and facilitated the attachment of Schwann cells. Further, increasing fiber density increased Schwann cell attachment and supported more neurite extension than when cultured on the low-density scaffolds. Crossing fibers seemed to divert neurite outgrowth and in some cases stopped neurite outgrowth from occurring. Future work is focusing on maintaining fiber alignment for *in vitro* and *in vivo* experimentation. Further, studies on how fiber density and fiber diameter influence neurite outgrowth in both *in vitro* and *in vivo* systems are also currently under way. The goal is to best construct scaffolds containing aligned, electrospun fibers for nerve regeneration applications.

Acknowledgments

This work was supported by grants from the Department of Energy, USA, and Seed and Infrastructure Enhancement Grants from Michigan Technological University. The authors would like to thank Dr P Heiden (MTU, Houghton, MI) for her suggestions on electrospinning, Dr D Clupper (MTU, Houghton, MI) and his student D Jaroch for assistance in designing the electrospinning set up, and Eric Minner for manuscript editing and assistance with statistics.

References

- Alexander J K, Fuss B and Colello R J 2006 Electric field-induced astrocyte alignment directs neurite outgrowth *Neuron Glia Biol.* **2** 93–103
- Ayres C, Bowlin G L, Henderson S C, Taylor L, Shultz J, Alexander J, Telemeco T A and Simpson D G 2006 Modulation of anisotropy in electrospun tissue engineering scaffolds: analysis of fiber alignment by the fast Fourier transform *Biomaterials* **27** 5524–34
- Baker B M, Gee A O, Metter R B, Nathan A S, Marklein R A, Burdick J A and Mauck R L 2008 The potential to improve cell infiltration in composite fiber-aligned electrospun scaffolds by the selective removal of sacrificial fibers *Biomaterials* **29** 2348–58
- Balgude A P, Yu X, Szymanski A and Bellamkonda R V 2001 Agarose gel stiffness determines rate of DRG neurite extension in 3D cultures *Biomaterials* **22** 1077–84
- Bilsland J, Migby M, Young L and Harper S 1999 A rapid method for semi-quantitative analysis of neurite outgrowth from chick DRG explants using image analysis *J. Neurosci. Methods* **92** 75–85
- Biran R, Noble M D and Tresco P A 2003 Directed nerve outgrowth is enhanced by engineered glial substrates *Exp. Neurol.* **184** 141–52
- Blits B, Kitay B M, Farahvar A, Caperton C V, Dietrich W D and Bunge M B 2005 Lentiviral vector-mediated transduction of neural progenitor cells before implantation into injured spinal cord and brain to detect their migration, deliver neurotrophic factors and repair tissue *Restor. Neurol. Neurosci.* **23** 313–24
- Cai J, Peng X, Nelson K D, Eberhard R and Smith G M 2005 Permeable guidance channels containing microfilament scaffolds enhance axon growth and maturation *J. Biomed. Mater. Res. A* **75** 374–86
- Ceballos D, Navarro X, Dubey N, Wendelschafer-Crabb G, Kennedy W R and Tranquillo R T 1999 Magnetically aligned collagen gel filling a collagen nerve guide improves peripheral nerve regeneration *Exp. Neurol.* **158** 290–300
- Chauhan N B, Figlewicz H M and Khan T 1999 Carbon filaments direct the growth of postlesional plastic axons after spinal cord injury *Int. J. Dev. Neurosci.* **17** 255–64
- Chew S Y, Mi R, Hoke A and Leong K W 2007 Aligned protein–polymer composite fibers enhance nerve regeneration: a potential tissue-engineering platform *Adv. Funct. Mater.* **17** 1288–96
- Chew S Y, Mi R, Hoke A and Leong K W 2008 The effect of the alignment of electrospun fibrous scaffolds on Schwann cell maturation *Biomaterials* **29** 653–61
- Chew S Y, Wen J, Yim E K F and Leong K W 2005 Sustained release of proteins from electrospun biodegradable fibers *Biomacromolecules* **6** 2017–24
- Choi J S, Lee S J, Christ G J, Atala A and Yoo J J 2008 The influence of electrospun aligned poly(epsilon-caprolactone)/collagen nanofiber meshes on the formation of self-aligned skeletal muscle myotubes *Biomaterials* **29** 2899–906
- Corey J M, Gertz C C, Wang B S, Birrell L K, Johnson S L, Martin D C and Feldman E L 2008 The design of electrospun PLA nanofiber scaffolds compatible with serum-free growth of primary motor and sensory neurons *Acta Biomater.* **4** 863–75
- Corey J M, Lin D Y, Mycek K B, Chen Q, Samuel S, Feldman E L and Martin D C 2007 Aligned electrospun nanofibers specify the direction of dorsal root ganglia neurite growth *J. Biomed. Mater. Res. A* **83** 636–45
- Deister C and Schmidt C E 2006 Optimizing neurotrophic factor combinations for neurite outgrowth *J. Neural Eng.* **3** 172–9
- Deizel J M, Kleinmeyer J, Harris D and Beck Tan N C 2001 The effect of processing variables on the morphology of electrospun nanofibers and textiles *Polymer* **42** 261–72
- Dodla M C and Bellamkonda R V 2006 Anisotropic scaffolds facilitate enhanced neurite extension *in vitro* *J. Biomed. Mater. Res. A* **78** 213–21
- Dodla M C and Bellamkonda R V 2008 Differences between the effect of anisotropic and isotropic laminin and nerve growth factor presenting scaffolds on nerve regeneration across long peripheral nerve gaps *Biomaterials* **29** 33–46
- Fong H, Chun I and Reneker D H 1999 Beaded nanofibers formed during electrospinning *Polymer* **40** 4585–92
- Fong H and Reneker D H 1999 Elastomeric nanofibers of styrene–butadiene–styrene triblock copolymer *J. Polym. Sci. B* **37** 3488–93
- Hadlock T, Sundback C, Hunter D, Cheney M and Vacanti J P 2000 A polymer foam conduit seeded with Schwann cells promotes guided peripheral nerve regeneration *Tissue Eng.* **6** 119–27
- Huang Z-M, Zhang Y Z, Kotaki M and Ramakrishna S 2003 A review on polymer nanofibers by electrospinning and their applications in nanocomposites *Compos. Sci. Technol.* **63** 2223–53

- Hurtado A, Moon L D F, Maquet V, Blits B, Jérôme R and Oudega M 2006 Poly (D, L-lactic acid) macroporous guidance scaffolds seeded with Schwann cells genetically modified to secrete a bi-functional neurotrophin implanted in the completely transected adult rat thoracic spinal cord *Biomaterials* **27** 430–42
- Johansson F, Carlberg P, Danielsen N, Montelius L and Kanje M 2006 Axonal outgrowth on nano-imprinted patterns *Biomaterials* **27** 1251–8
- Kim I A, Park S A, Kim Y J, Kim S H, Shin H J, Lee Y J, Kang S G and Shin J W 2005 Effects of mechanical stimuli and microfiber-based substrate on neurite outgrowth and guidance *J. Biosci. Bioeng.* **101** 120–6
- Kim Y T, Haftel V K, Kumar S and Bellamkonda R V 2008 The role of aligned polymer fiber-based constructs in the bridging of long peripheral nerve gaps *Biomaterials* **29** 3117–27
- Levi A D, Bunge R P, Lofgren J A, Meima L, Hefti F, Nikolic K and Sliwkowski M X 1995 The influence of heregulins on human Schwann cell proliferation *J. Neurosci.* **15** 1329–40
- Loeb J E, Cordier W S, Harris M E, Weitzman M D and Hope T J 1999 Enhanced expression of transgenes from adeno-associated virus vectors with the woodchuck hepatitis virus posttranscriptional regulatory element: implications for gene therapy *Hum. Gene Ther.* **10** 2295–305
- Manwaring M E, Walsh J F and Tresco P A 2004 Contact guidance induced organization of extracellular matrix *Biomaterials* **25** 3631–8
- Matthews G G 1998 Generation of nerve action potentials *Cellular Physiology of Nerve and Muscle* (Malden: Blackwell Science) pp 61–94
- Morrissey T K, Kleitman N and Bunge R P 1991 Isolation and functional characterization of Schwann cells derived from adult peripheral nerve *J. Neurosci.* **11** 2433–42
- Naldini L, Blomer U, Gage F H, Trono D and Verma I M 1996 Efficient transfer, integration, and sustained long-term expression of the transgene in adult rat brains injected with a lentiviral vector *Proc. Natl Acad. Sci. USA* **93** 11382–8
- Ngo T-T B, Waggoner P J, Romero A A, Nelson K D, Eberhart R C and Smith G M 2003 Poly(L-lactide) microfilaments enhance peripheral nerve regeneration across extended nerve lesions *J. Neurosci. Res.* **72** 227–38
- Pan H, Li L, Hu L and Cui X 2006 Continuous aligned polymer fibers produced by a modified electrospinning method *Polymer* **47** 4901–4
- Prang P, Miller R, Eljaouhari A, Heckmann K, Kunz W, Weber T, Faber C, Vroemen M, Bogdahn U and Weidner N 2006 The promotion of oriented axonal regrowth in the injured spinal cord by alginate-based anisotropic capillary hydrogels *Biomaterials* **27** 3560–9
- Rangappa N, Romero A, Nelson K D, Eberhard R C and Smith G M 2000 Laminin-coated poly(L-lactide) filaments induce robust neurite growth while providing directional orientation *J. Biomed. Mater. Res.* **51** 625–34
- Rutledge G C and Fridrikh S V 2007 Formation of fibers by electrospinning *Adv. Drug Deliv. Rev.* **59** 1384–91
- Rydmark M 1981 Nodal axon diameter correlates linearly with intermodal axon diameter in spinal roots of the cat *Neurosci. Lett.* **24** 247–50
- Shah A, Fischer C, Knapp C F and Sisken B F 2004 Quantification of neurite growth parameters in explants cultures using a new image processing program *J. Neurosci. Methods* **136** 123–31
- Stokols S and Tuszyński M H 2006 Freeze-dried agarose scaffolds with uniaxial channels stimulate and guide linear axonal growth following spinal cord injury *Biomaterials* **27** 443–51
- Teo W E, Kotaki M, Mo X M and Ramakrishna S 2005 Porous tubular structures with controlled fibre orientation using a modified electrospinning method *Nanotechnology* **16** 918–24
- Wen X and Tresco P A 2006 Effect of filament diameter and extracellular matrix molecule precoating on neurite outgrowth and Schwann cell behavior on multifilament entubulation bridging device *in vitro* *J. Biomed. Mater. Res. A* **76** 626–37
- Xu C Y, Inai R, Kotaki M and Ramakrishna S 2004 Aligned biodegradable nanofibrous structure: a potential scaffold for blood vessel engineering *Biomaterials* **25** 877–86
- Yang F, Murugan R, Wang S and Ramakrishna S 2005 Electrospinning of nano/micro scale poly(L-lactic acid) aligned fibers and their potential in neural tissue engineering *Biomaterials* **26** 2603–10
- Yang F, Xu C Y, Kotaki M, Wang S and Ramakrishna S 2004 Characterization of neural stem cells on electrospun poly(L-lactic acid) nanofibrous scaffold *J. Biomater. Sci. Polym. Ed.* **15** 1483–97